

Numerical studies on detonation propagation in inhomogeneous mixtures with periodic reactant concentration gradient

Yuan Wang^{1,2}, Chengyang Huang², Ralf Deiterding³, Haitao Chen¹ and Zheng Chen^{2,†}

¹Institute of Applied Physics and Computational Mathematics, Beijing 100094, PR China

²SKLTCS, CAPT, BIC-ESAT, College of Engineering, Peking University, Beijing 100871, PR China

³Aerodynamics and Flight Mechanics Research Group, University of Southampton, Boldrewood Campus, Southampton SO16 7QF, UK

(Received 7 November 2021; revised 17 October 2022; accepted 14 December 2022)

In detonation engines and accidental explosions, a detonation may propagate in an inhomogeneous mixture with non-uniform reactant concentration. In this study, one- and two-dimensional simulations are conducted for detonation propagation in hydrogen/oxygen/nitrogen mixtures with periodic sinusoidal or square wave distribution of the reactant concentration. The objective is to assess the properties of detonation propagation in such inhomogeneous mixtures. Specifically, detonation quenching and reinitiation, cellular structure, cell size and detonation speed deficit are investigated. It is found that there exists a critical amplitude of the periodic mixture composition distribution, above which the detonation quenches. When the amplitude is below the critical value, detonation quenching and reinitiation occur alternately. A double cellular structure consisting of substructures and a large-scale structure is found for a two-dimensional detonation propagating in inhomogeneous mixtures with a periodic reactant concentration gradient. The detonation reinitiation process and the formation of the double cellular structure are interpreted. To quantify the properties of detonation propagation in different inhomogeneous mixtures, the large cell size, critical amplitude, transition distance and detonation speed deficit are compared for hydrogen/air without and with nitrogen dilution and for periodic sine wave and square wave distributions of the reactant concentration. The large-scale cell size is found to be linearly proportional to the wavelength, and both the critical amplitude and the transition distance decrease with the wavelength. The small detonation speed deficit is shown to be due to the incomplete combustion of the reactant. This work provides helpful understanding of the features of detonation propagation in inhomogeneous mixtures.

Key words: combustion, detonations

† Email address for correspondence: cz@pku.edu.cn

1. Introduction

In detonation engines, a detonation may propagate in inhomogeneous gaseous mixtures since fuel and oxidizer are usually injected separately into the combustion chamber and it is difficult for them to be perfectly mixed (Lu & Braun 2014; Fujii *et al.* 2017). In accidental explosions, detonation initiation and quenching also occur in non-uniform mixtures (Boulal, Vidal & Zitoun 2016). Therefore, there is increasing interest in studying detonation propagation in inhomogeneous gaseous mixtures.

Generally, six typical distributions of inhomogeneous mixtures, as depicted in figure 1, have been considered so far. Figures 1(a) and 1(b) show reactants with fuel concentration gradient normal (Ishii & Kojima 2007; Lieberman & Shepherd 2007a,b; Kessler, Gamezo & Oran 2012; Ettner, Vollmer & Sattelmayer 2013; Boeck *et al.* 2015; Grune *et al.* 2017; Khodadadi Azadboni *et al.* 2019; Zheng *et al.* 2019) and parallel (Thomas, Sutton & Edwards 1991; Kuznetsov *et al.* 1998; Boulal *et al.* 2016, 2018; Ma, Wang & Han 2020) to the detonation propagation direction, respectively. Figures 1(c) and 1(d) depict reactants with inert layers parallel (Houim & Fievisohn 2017; Reynaud, Virost & Chinnayya 2017; Maxwell & Melguizo-Gavilanes 2019; Taileb, Melguizo-Gavilanes & Chinnayya 2019) and normal (Gavrilenko, Krasnov & Nikolaev 1982; Bjerketvedt, Sonju & Moen 1986; Teodorczyk & Benoan 1996; Kuznetsov *et al.* 1997; Li *et al.* 2008; Fujii *et al.* 2017; Ishii & Seki 2017; Peace & Lu 2017; Tang *et al.* 2017; Peace & Lu 2018; Tang *et al.* 2018; Chen, Liu & Wang 2019; Tang *et al.* 2019a,b) to the detonation propagation direction, respectively. Similar to the case in figure 1(d), several studies (Kuznetsov *et al.* 1997; Li *et al.* 2008; Peace & Lu 2017; Tang *et al.* 2017; Peace & Lu 2018; Tang *et al.* 2018; Tang *et al.* 2019a,b) have investigated the detonation transmission across the interface for density, temperature or mixture composition. Besides, detonation propagation in mixtures with uniformly or randomly distributed inert regions or in a porous medium (see figure 1e) has also been investigated previously (Lieberman & Shepherd 2007a,b; Radulescu & Maxwell 2011; Li, Mi & Higgins 2015; Gaathaug, Vaagsaether & Bjerketvedt 2017; Mi *et al.* 2017a; Mi, Timofeev & Higgins 2017b; Mi *et al.* 2019; Prakash & Raman 2019).

In this study we consider the detonation propagation in inhomogeneous mixtures with periodic fuel concentration gradient parallel to the detonation propagation direction, as depicted in figure 1(f). In rotating detonation engines, the unburned reactants are injected into the combustion chamber through injection ports and burned gas might exist at the injection-port intervals (Fujii *et al.* 2017). In accidental explosions, the injection of water and inert gas is used to disperse the continuous distribution of combustible gas (Teodorczyk & Benoan 1996). Therefore, in both rotating detonation engines and accidental explosions, a detonation might propagate in inhomogeneous mixtures as depicted in figure 1(f). However, in the literature there are only a few studies on detonation propagation in this type of inhomogeneous mixture. Thomas *et al.* (1991) experimentally investigated the detonation propagation in mixtures with concentration gradient and found that the transmitted detonation adjusts its speed and cell size rapidly to the local gas composition. Kuznetsov *et al.* (1998) conducted experiments on detonation transmission in non-uniform mixtures and found that the detonation propagation is significantly affected by the magnitude of the concentration gradient. Boulal *et al.* (2016, 2018) experimentally investigated detonation quenching and reinitiation in non-uniform compositions and proposed a criterion to quantify shock–reaction zone decoupling. Due to the difficulty in preparing non-uniform reactants and measuring composition distribution in experiments, simulations were conducted in previous studies. In their one-dimensional (1-D) simulations, Ma *et al.* (2020) found that a periodic gradient

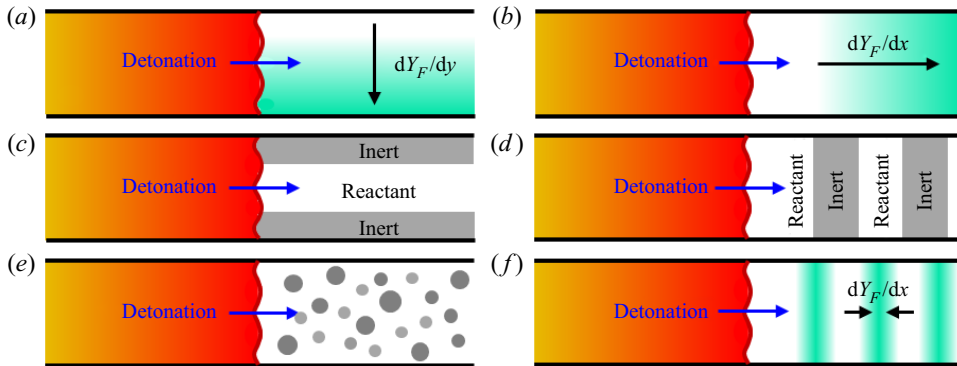


Figure 1. Schematic of detonation propagating in different inhomogeneous mixtures. The white and grey regions represent reactants and inert, respectively. The light green colour represents higher reactant concentration.

in reactant concentration affects detonation propagation modes and that composition inhomogeneity helps to stabilize a pulsating detonation under certain conditions. Mi *et al.* (2017a) studied gaseous detonation propagation in non-uniform mixtures and found that the averaged detonation propagation speed in an inhomogeneous mixture is higher than that in a homogeneous mixture. Radulescu & Maxwell (2011) experimentally and numerically investigated the detonation propagating through a porous medium and found that wave diffraction and reflection are critical mechanisms for detonation attenuation and reinitiation.

However, most of the previous studies considered detonation propagation in mixtures with a single concentration gradient. Detonation propagation in inhomogeneous mixtures with a periodic gradient in reactant concentration has received little attention. Besides, although 1-D simulation results were reported by Ma *et al.* (2020), the evolution of cellular detonation structure was not studied before.

Based on the above considerations, here we consider detonation propagation in inhomogeneous $H_2/O_2/N_2$ mixtures with a periodic gradient in reactant concentration. Both 1-D and two-dimensional (2-D) simulations considering detailed chemistry have been conducted. The objective of this study is to assess the effects of a periodic gradient in reactant concentration on detonation propagation properties, including detonation quenching and reinitiation, cellular structure, cell size and detonation speed deficit. This paper is structured as follows. Section 2 presents the numerical model and methods. Then, the evolution of 1-D and 2-D detonation propagation in inhomogeneous mixtures is investigated and the effects of the inhomogeneous mixture on detonation quenching and reinitiation and cellular structure are assessed in § 3. Finally, the conclusions are presented in § 4.

2. Numerical model and methods

We consider 1-D and 2-D detonation propagation in a stoichiometric $H_2/O_2/N_2$ mixture initially at $T_0 = 300$ K and $P_0 = 1$ atm. The numerical model is depicted in figures 1(f) and 2.

First, the detonation propagates through the static homogeneous $H_2/O_2/N_2$ mixture, whose molar ratio is $H_2 : O_2 : N_2 = 2 : 1 : s$. Table 1 lists the two types of mixtures for stoichiometric H_2 /air without ($s = 3.76$) and with ($s = 7$) nitrogen dilution, respectively.

Mixture	Molar ratio	Induction length, l_i (mm)
mixture 1	$H_2 : O_2 : N_2 = 2 : 1 : 3.76$	0.19
mixture 2	$H_2 : O_2 : N_2 = 2 : 1 : 7$	1.25

Table 1. Two types of mixtures initially at $T_0 = 300$ K and $P_0 = 1$ atm.

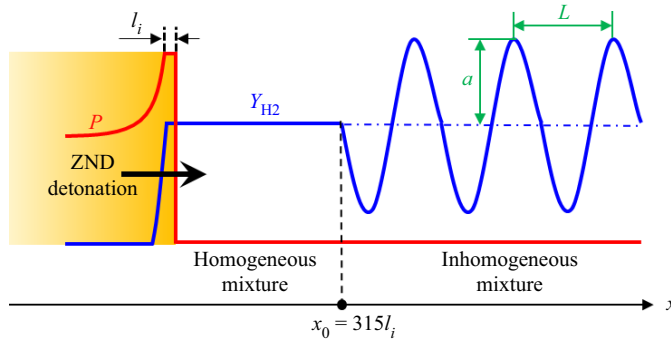


Figure 2. Schematic of the initial pressure and hydrogen mass fraction distributions.

Nitrogen dilution was introduced to mixture 2 to change the reactivity and the detonation properties including detonation speed and cell size. The induction length, l_i , and cell size, λ , for these two mixtures are listed in table 1. The cellular structure becomes steady and the cell size gradually increases as the detonation propagates forward. Considering the computational cost, the length of the homogeneous mixture is $x_0 = 421l_i$ for 1-D cases and $315l_i$ for 2-D cases, which was chosen to ensure quasi-steady detonation with constant cellular structure for the 2-D case. As shown in figure 2, the static inhomogeneous mixture has a sinusoidal distribution of mixture composition and the molar fraction of each species is

$$\left. \begin{aligned} x_{H_2} &= \{2 - 2 \times a \times \sin[2\pi(x - x_0)/L]\}/(2 + 1 + s), \\ x_{O_2} &= \{1 - 1 \times a \times \sin[2\pi(x - x_0)/L]\}/(2 + 1 + s), \\ x_{N_2} &= \{s + 3 \times a \times \sin[2\pi(x - x_0)/L]\}/(2 + 1 + s), \end{aligned} \right\} \quad (2.1)$$

where L is the wavelength and a is the amplitude of the sinusoidal distribution as depicted in figure 2. Equation (2.1) indicates that the molar ratio between hydrogen and oxygen is 2 everywhere and that the averaged fuel molar concentration in the inhomogeneous mixture is the same as that in the homogeneous mixture. Different values for L in the range of 1–16 mm and for a in the range of 0–1 were considered. The homogeneous mixture is recovered for $a = 0$. Note that in the homogeneous and inhomogeneous unburned mixtures, the temperature and pressure are respectively 300 K and 1 atm everywhere. The density depends on the mixture composition and has sinusoidal distribution in the inhomogeneous mixture.

The in-house code A-SURF (Chen 2010; Dai & Chen 2015) and the parallel block-structured mesh refinement framework AMROC (Deiterding 2009) were

respectively used to simulate the 1-D and 2-D detonation propagation in the inhomogeneous $\text{H}_2/\text{O}_2/\text{N}_2$ mixtures. The conservation equations for unsteady, multicomponent, compressible, reactive flows were solved in both A-SURF and AMROC using the finite-volume approach. Diffusion terms were kept in the conservation equations. The temporal integration, convective fluxes and diffusive fluxes were calculated, respectively, using the Runge–Kutta, MUSCL-Hancock and central difference schemes in A-SURF (Chen 2010; Dai & Chen 2015). For AMROC, a hybrid Roe-HLL Riemann solver for mixtures of thermally perfect gases was used to calculate the convective fluxes. The central difference scheme was used for the diffusion terms (Deiterding 2009). The detailed chemistry for hydrogen developed by Li *et al.* (2004) was used. When a detailed chemistry rather than one-step chemistry is considered, there exists a so-called crossover temperature, below which the intermediate/radical is removed from the system by chain-termination reactions too quickly for a chain-branching process to occur. The CHEMKIN packages were incorporated into A-SURF and AMROC to evaluate the temperature- and component-dependent thermodynamic and transport properties as well as the reaction rates. The mixture-averaged model was used for diffusion, and the Soret and Dufour effects were not included in this study. Details on diffusion terms and related discussion can be found in § 3 of the supplementary material available at <https://doi.org/10.1017/jfm.2022.1074>. The VODE solver (Brown, Byrne & Hindmarsh 1989) and the semi-implicit Runge–Kutta method GRK4A were adopted to integrate stiff reaction terms in A-SURF and AMROC, respectively. The Godunov splitting method was used to decouple hydrodynamic transport and the stiff chemical reaction source terms numerically. A-SURF and AMROC have successfully been used in previous studies to simulate detonation initiation and propagation (Deiterding 2009; Deiterding 2011; Dai & Chen 2015; Qi & Chen 2017; Wang *et al.* 2018; Dai & Chen 2019; Huang, Qi & Chen 2019). The details of the governing equations and numerical schemes of A-SURF and AMROC can be found in Chen (2010), Dai & Chen (2015) and Wang *et al.* (2018) and therefore are not repeated here.

The computational domains are $0 \leq x \leq 60$ cm in 1-D simulations and $0 \leq x \leq 60$ cm and $0 \leq y \leq 4$ cm in 2-D simulations. The length of 60 cm was chosen to ensure that in the inhomogeneous region the quasi-steady-state propagation can be reached and the detonation structure can fully develop. The chosen domain width of 4 cm is large enough to guarantee the independence of cell size with domain width in 2-D simulations. On the left- and right-hand sides of the computational domain in both 1-D and 2-D simulations, adiabatic, reflective, no-slip wall boundary conditions were used. For the top and bottom sides in 2-D simulations, periodic boundary conditions were enforced and thereby boundary layer effects on detonation propagation were circumvented (Han, Gao & Law 2017). The ideal strong blast wave was used as the initial condition for 1-D simulations (Qi & Chen 2017). For 2-D simulations, the ZND detonation structure was used and the position of peak pressure is $x = 1$ cm and thus the expansion wave does not affect the leading shock propagation due to the backwall condition. To accurately and efficiently resolve the detonation propagation, dynamically adaptive mesh refinement was used in both A-SURF and AMROC. Mesh refinement or coarsening was determined by the local gradients of temperature, pressure and density. The base mesh size was 250 μm . After six level mesh refinement, the finest mesh size was around 3.9 μm . Since the detonation induction length is 0.19 mm, there were around 50 grid points within an induction length. The detonation propagation was adequately resolved and grid convergence was ensured, which was demonstrated through comparing results predicted by different finest mesh sizes (see figure A1 in the supplementary material).

3. Results and discussion

3.1. One-dimensional detonation propagation

First, we consider 1-D detonation propagation in a stoichiometric H_2/air mixture (i.e. mixture 1 with $s = 3.76$) with the periodic sinusoidal wave distribution of reactant concentration. Different values of wavelength L and amplitude a were considered, and the effects of periodic mixture composition distribution on 1-D detonation propagation were examined. It is noted that the 1-D Chapman–Jouguet (CJ) detonation in a stoichiometric H_2/air mixture is unstable and exhibits pulsating instabilities (Daimon & Matsuo 2007). The stability depends on the ratio between the imposed detonation velocity and the CJ velocity (i.e. the degree of overdrive). It also depends sensitively on the activation energy, as well as on the heat release and specific heat ratio. At higher overdrive (velocity larger than the CJ value), the detonation becomes stable. In this work, the detonation initiation is an overdriven state due to the employment of an ideal strong blast wave. After initiation, oscillation-free detonation propagation occurs around $5 < x < 25$ cm. Moreover, as the overdriven detonation propagates forward, the speed of the leading shock wave decreases rapidly and recovers to CJ speed at $x > 8$ cm. In order to exclude the effects of aforementioned pulsating instabilities and overdriven state of detonation on detonation propagation through inhomogeneous mixtures, the lengths of homogeneous and inhomogeneous regions were set to be 8 and 18 cm, respectively.

We first fix the wavelength to be $L = 16$ mm. Figure 3 shows the evolution of pressure after the shock and the lead shock speed for three amplitudes of $a = 0.2, 0.5$ and 0.8 . The dashed black lines correspond to the results calculated based on initial local reactant concentration given by (2.1). Specifically, we calculated a 1-D steady detonation by Cantera (Goodwin, Moffat & Speth 2016) and obtained the variations of the pressure after the shock (i.e. von Neumann spike pressure) in figure 3(a) and CJ speed in figure 3(b) with the initial local reactant concentration given by (2.1). The number, n , from 1 to 7, represents the n th period of sinusoidal distribution of mixture composition. The minus and plus represent, respectively, lower and higher chemical reactivity than the homogeneous mixture (see figure 2).

In the homogeneous region at $x < x_s = 8$ cm, the detonation propagates at CJ speed of $S_{SHOCK} = V_{CJ} = 1975 \text{ m s}^{-1}$, and the leading shock pressure is equal to that of the von Neumann state, i.e. $P_S = P_{VN} = 24.9$ atm. In the inhomogeneous mixture with amplitude of $a = 0.2$, the detonation propagates with periodic fluctuations of pressure after the shock. The leading shock pressure changes from $P_S = 23.5$ atm at $x = 8.4$ cm with the lowest fuel concentration to $P_S = 25.7$ atm at $x = 9.2$ cm with the highest fuel concentration. The detonation propagates successfully in the inhomogeneous mixture, and its speed agrees well with the local CJ speed. Therefore, as expected, a low-amplitude disturbance in reactant concentration has little effect on detonation propagation.

When the amplitude is increased to $a = 0.5$, detonation quenching and reinitiation occur. The shock pressure decreases from $P_S = P_{VN} = 24.9$ atm at $x = 8.0$ cm to $P_S = 15.2$ atm at $x = 8.8$ cm due to the relatively low concentration of H_2/O_2 in the first inhomogeneous region 1– ($8.0 < x < 8.8$ cm). The leading shock decouples from the reaction front and thereby the detonation quenches. When the leading shock propagates into region 1+ ($8.8 < x < 9.6$ cm) with relatively high concentration of H_2/O_2 , local autoignition occurs around $x = 9.2$ cm. Consequently, the reaction front accelerates and catches up and couples with the leading shock, resulting in an overdriven detonation with $P_S = 70$ atm and $S_{SHOCK} = 2766 \text{ m s}^{-1}$. The detailed origins of this detonation quenching and reinitiation process are interpreted in figure 4. From region 2 to region 7, the shock pressure and shock speed are shown to change periodically with the sinusoidal distribution in reactant

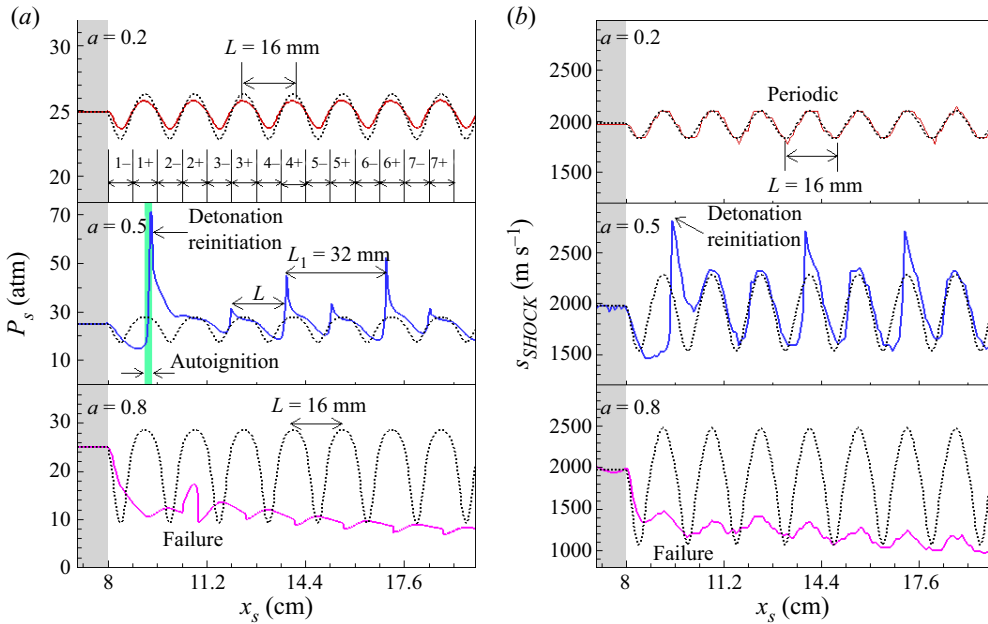


Figure 3. Change of (a) the pressure after the shock, P_s , and (b) leading shock speed, S_{SHOCK} , with the shock position, X_s , for a fixed wavelength of $L = 16$ mm but different amplitudes of $a = 0.2, 0.5$ and 0.8 in mixture 1. The dashed black lines correspond to (a) the pressure at the von Neumann state and (b) the CJ speed calculated based on the initial local reactant concentration given by (2.1).

concentration at a wavelength of $L = 16$ mm. Moreover, after the detonation reinitiation is achieved, the variations of shock pressure and shock speed become regular and consecutive peaks appear at a constant distance of $L_1 = 2L = 32$ mm.

When the amplitude is further increased to $a = 0.8$, figure 3(b) shows that the shock speed attenuates from $S_{SHOCK} = V_{CJ} = 1975$ m s⁻¹ for $x < 8.0$ cm to $S_{SHOCK} = 1366$ m s⁻¹ at $x = 8.6$ cm in region 1-. The shock is too weak to trigger local autoignition/explosion in region 1+ with relatively high concentration of H₂/O₂. Consequently, the detonation quenches without reinitiation. Therefore, for each wavelength there is a critical amplitude, denoted as a_c , below which the detonation can propagate successfully in the inhomogeneous mixture.

To interpret the detonation quenching and reinitiation observed in the inhomogeneous mixture, the temporal evolutions of pressure, temperature and heat release rate distributions for $a = 0.5$ are shown in figure 4(a). In region 1- with $8.0 < x < 8.8$ cm (i.e. $38.7 < t < 43.7$ μs), the pressure peak behind the leading shock immediately decreases from $P_s = P_{VN} = 24.9$ atm to $P_s = 15.2$ atm due to the relatively low H₂/O₂ concentration. Both the temperature and heat release rate behind the leading shock gradually decrease. At $t = 43.7$ μs, the distance between the leading shock and reaction front is around 0.9 mm, which is much larger than the induction length of $l_i = 0.19$ mm. The decoupling between the leading shock and reaction zone indicates that the detonation quenches. When the leading shock propagates into region 1+ with $8.8 < x < 9.6$ cm (i.e. $43.7 < t < 48.3$ μs) with relatively high H₂/O₂ concentration, local autoignition occurs around $t = 46.3$ μs after the reactants are compressed by the leading shock. The pressure wave generated by heat release from this local autoignition accelerates the propagation of the reaction front.

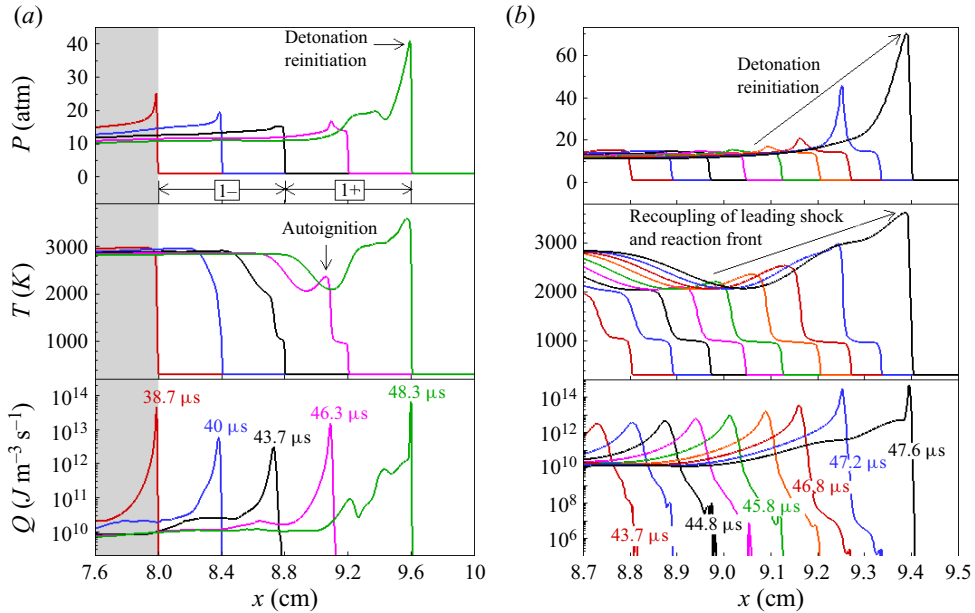


Figure 4. Temporal evolution of the pressure, temperature and heat release rate distributions during the first sinusoidal period for $L = 16$ mm and $a = 0.5$ in mixture 1.

At the end of region 1^+ ($t = 48.3 \mu\text{s}$ and $x = 9.6$ cm), the reaction front couples with the leading shock, resulting in an overdriven detonation with peak pressure around 40 atm.

Figure 4(b) further shows the details of the processes of autoignition and detonation reinitiation in region 1^+ . During $43.7 < t < 45.8 \mu\text{s}$, the leading shock pressure, temperature and heat release rate around the reaction front remain nearly constant. At $t = 45.8 \mu\text{s}$, due to the relatively high concentration of H_2/O_2 after the leading shock, local autoignition starts to occur, as indicated by the local pressure rise around $x = 9.2$ cm. The coherent enhancement between pressure wave and chemical reaction further increases the local heat release rate and pressure rise. On the other hand, in the region $9.2 < x < 9.4$ cm, the reactant concentration decreases from ($Y_{\text{H}_2} = 0.41, Y_{\text{O}_2} = 0.051$) to ($Y_{\text{H}_2} = 0.34, Y_{\text{O}_2} = 0.043$), which results in the spatial distribution of ignition delay time. According to the gradient theory by Zeldovich (1980), detonation development can occur during the reaction front propagation in this region. Consequently, a strong local autoignition/explosion occurs around $t = 47.2 \mu\text{s}$, after which an overdriven detonation is developed around $t = 47.6 \mu\text{s}$. A similar phenomenon was observed by Qi *et al.* (2017) for detonation development caused by concentration non-uniformity.

For the above results, the wavelength for the periodic sinusoidal mixture composition distribution were fixed to be $L = 16$ mm while the amplitude changes. We also considered a fixed amplitude of $a = 0.8$ but different wavelengths of $L = 2, 4, 8$ and 16 mm. The results are shown in figure 5. For $L = 2, 4$ and 8 mm, successful detonation reinitiation is achieved at the end of region 1^+ . However, detonation failure is observed for $L = 16$ mm. Therefore, for a given amplitude, detonation reinitiation can occur only for relatively small wavelengths. This is reasonable since longer shock decay occurs for longer wavelengths. Moreover, the double period propagation of the leading shock pressure is observed in figure 5 for all the cases that exhibit detonation reinitiation. A similar phenomenon is also found in the 2-D simulations presented later.

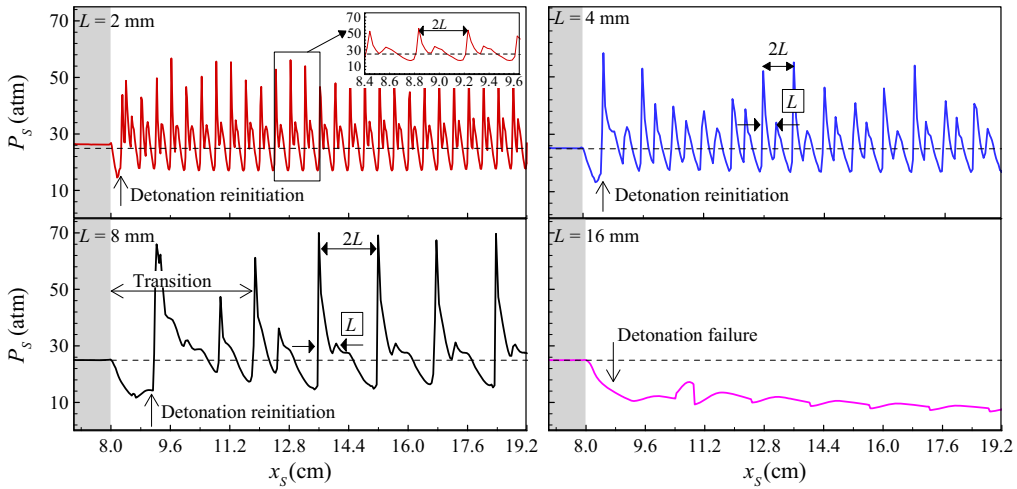


Figure 5. Change of the pressure after the shock, P_S , with the shock position, x_S , for a fixed amplitude of $a = 0.8$ but different wavelengths of $L = 2, 4, 8$ and 16 mm in mixture 1. The dashed black lines correspond to the pressure at the von Neumann state calculated based on the homogeneous mixture.

For successful detonation propagation in the inhomogeneous mixture, the detonation speed changes periodically as shown in figure 3. Here we assess how the sinusoidal mixture distribution affects the averaged detonation speed. Note that the mixture composition given by (2.1) ensures that the averaged fuel concentration in the inhomogeneous mixture is the same as that in the homogeneous mixture, for which the CJ speed is $V_{CJ} = 1975 \text{ m s}^{-1}$. Figure 6 shows the averaged detonation propagation speed for different values of wavelength and amplitude of sinusoidal mixture distribution. It is observed that the periodic sinusoidal distribution of mixture composition has little influence (within 3 %) on the averaged detonation propagation speed once the successful detonation reinitiation is achieved in the inhomogeneous mixture. The averaged detonation speed deficit is shown to be smaller for shorter wavelength and smaller amplitude. Such a small detonation speed deficit is due to the incomplete consumption of the fuel and oxidizer during the detonation propagation in the inhomogeneous mixture, which also occurs in 2-D simulations (see figures 16 and 17 and related discussion). A similar detonation speed deficit was also reported by Calhoun & Sinha (2005), Kessler *et al.* (2012), Boeck *et al.* (2015) and Han, Wang & Law (2019).

3.2. Two-dimensional detonation propagation

In this subsection, we consider 2-D detonation propagation in inhomogeneous mixtures with periodic reactant concentration gradient. First, detonation reinitiation and double cellular structure in an inhomogeneous stoichiometric H_2/air mixture are considered. Then, the effects of mixture composition and concentration distribution are assessed. Finally, the large cell size, quenching condition and detonation speed deficit are discussed.

3.2.1. Detonation reinitiation and double cellular structure

Figure 7 shows the numerical soot foils for a fixed wavelength of $L = 2$ mm but different amplitudes in the range of $a = 0-0.7$. The inhomogeneous region starts at $x_S = 6$ cm, which corresponds to the vertical dashed black line in figure 7. The numerical soot foil

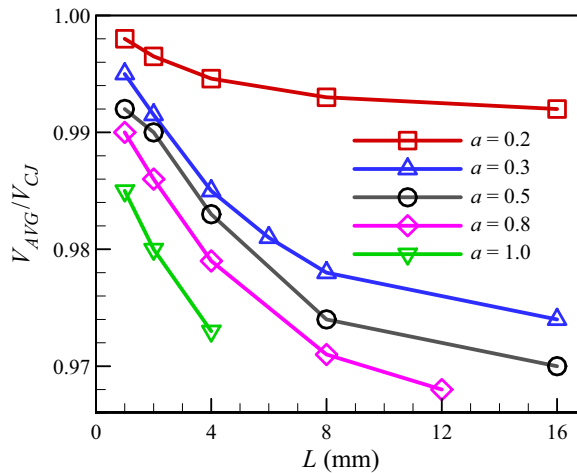


Figure 6. Change of the normalized averaged detonation propagation speed, V_{AVG}/V_{CJ} , with the wavelength, L , for different amplitudes of $a = 0.2, 0.3, 0.5, 0.8$ and 1.0 in mixture 1.

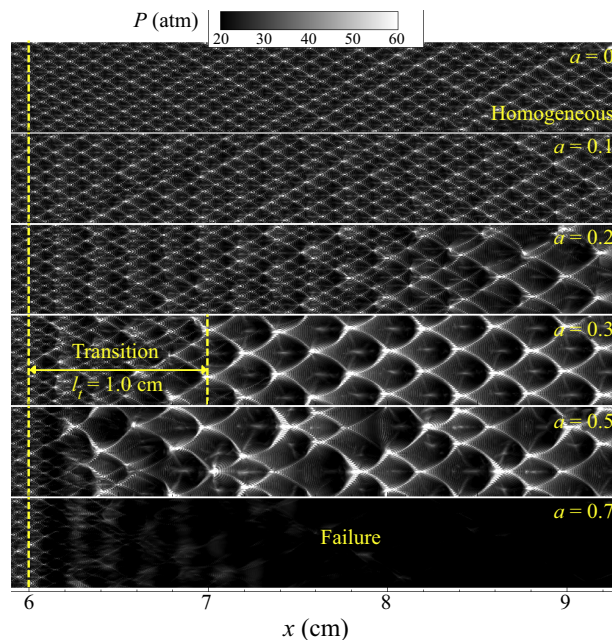


Figure 7. Numerical soot foils for a fixed wavelength of $L = 2$ mm and different amplitudes of $a = 0, 0.1, 0.2, 0.3, 0.5$ and 0.7 in mixture 1.

is plotted by recording the maximum pressure reached at each grid point of the numerical domain. In the numerical soot foil, the pressure record is plotted on a linear grey scale with black/white colour corresponding to minimum/maximum pressure.

It is noted that the cell size gradually increases as the detonation propagates forward (see figure 7), even at $x = 12$ cm (see A2 in the supplementary material). This is because the initiated detonation is in an overdriven state and it first undergoes a decaying process

and then gradually approaches the self-sustained propagation process. Due to the limit of computational cost, the length of the homogeneous and inhomogeneous regions cannot be very large. Consequently, this study was performed in a region where the detonation is still undergoing decay from its initially overdriven state, and thereby the corresponding results and conclusions were based on this consideration.

For the homogeneous mixture with $a = 0$, the detonation propagates at the CJ speed, and regular cellular structure develops. The cell size (height in the vertical direction) is $\lambda_0 = 0.833$ mm and the cell length (width in the horizontal direction) is $w_0 = 1.66$ mm at $x = 6$ cm. For the inhomogeneous mixture with $a = 0.1$, the cellular structure is nearly the same as that for $a = 0$. This indicates that a small perturbation in the reactant concentration has little effect on the detonation propagation. For $a = 0.2, 0.3$ and 0.5 , a much larger cellular structure appears in the inhomogeneous region. The size of the large cellular structure does not change with the amplitude and it remains around $\lambda = 2.5$ mm. Before the appearance of the quasi-steady large-scale cellular structure, there is a transition region starting from $x_s = 6$ cm. Figure 7 shows that the transition distance is around $l_t = 1.0$ cm for $a = 0.3$. The transition distance is shown to decrease with amplitude and is discussed later in figure 15. When the amplitude is further increased to $a = 0.7$, the detonation quenches in the inhomogeneous region and the cellular structure gradually disappears. Therefore, similar to the 1-D case, there is also a critical amplitude, a_c , above which the 2-D detonation quenches in the inhomogeneous mixture. It is noted that the results only for $x < 9.3$ cm are shown in figure 7. The cellular structure does not change for $x > 9$ cm and $a = 0.3$ (see figure A3 in the supplementary material).

Figure 8 compares the numerical soot foils for a fixed amplitude of $a = 0.3$ but different wavelengths of $L = 1, 2$ and 4 cm. It is observed that the size of large-scale cells in the inhomogeneous region (i.e. $x > 6$ cm) increases with the wavelength. For $L = 4$ mm, the large cell size is around $\lambda = 5$ mm, which is one order of magnitude larger than $\lambda_0 = 0.833$ mm for the homogeneous mixture. A further increase of the wavelength to $L = 16$ cm leads to detonation quenching in the inhomogeneous mixture for $a = 0.3$ (not shown here). Therefore, for each amplitude there is a critical wavelength, denoted as L_c , above which the detonation quenches in the inhomogeneous mixture. In addition, the influence of the periodic boundary conditions used in the present 2-D simulations was also investigated. To exclude the effect of periodic boundary conditions on the cellular structure, we calculated the case for a wavelength of $L = 4$ and amplitude of $a = 0.3$ at the same condition except using slip wall boundary conditions for the top and bottom sides instead of periodic boundary conditions. The results show that the large cell size is slightly smaller than for the results obtained when using periodic boundary conditions, but the transition processes are consistent, including the double cellular structure stage. This indicates that the use of periodic boundary condition is suitable.

Furthermore, figure 8 shows that substructures appear within the large cellular structure in the range of $6.5 < x < 8$ cm for $L = 4$ mm. A similar phenomenon has been found in 1-D simulations with double periodic propagation of the leading shock pressure (see figures 3 and 5 with $L_1 = 2L$). This is also similar to the double cellular structure appearing in a gaseous nitromethane/air mixture due to two-stage heat release rather than mixture composition non-uniformity (Presles *et al.* 1996).

In order to interpret the double cellular structure, the numerical soot foils and leading shock pressure for $L = 8$ mm and $a = 0.3$ are plotted in figure 9. As described for the 1-D simulations, the number, n , from 1 to 7, represents the n th period of sinusoidal distribution of mixture composition, and the minus and plus represent respectively lower and higher chemical reactivity than the homogeneous mixture (see figure 2).

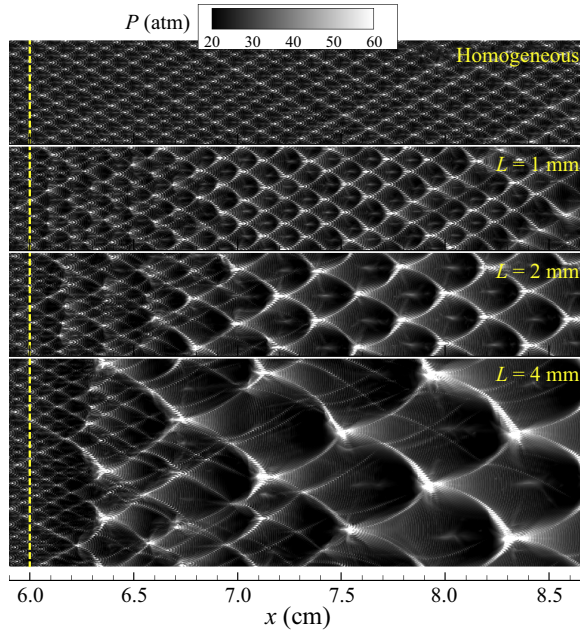


Figure 8. Numerical soot foils for a fixed amplitude of $a = 0.3$ and different wavelengths of $L = 1, 2$ and 4 mm in mixture 1. The results for the homogeneous mixture (i.e. $a = 0$) are shown together for comparison.

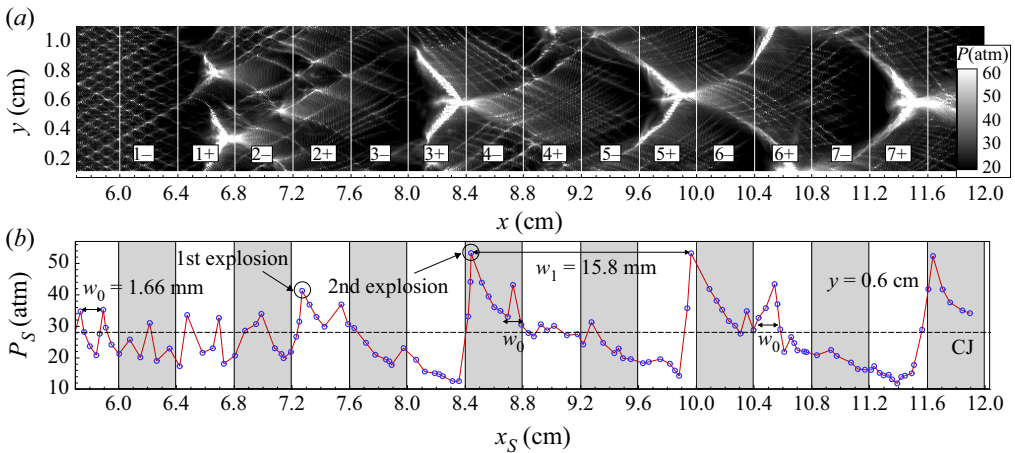


Figure 9. (a) Numerical soot foils and (b) change of the pressure immediately after the leading shock, P_S , with the shock position, x_S , along the line at $y = 0.6$ cm for $L = 8$ mm and $a = 0.3$ in mixture 1.

In the homogeneous mixture (i.e. $x < 6$ cm), the original cellular structure with height of $\lambda_0 = 0.833$ mm and length of $w_0 = 1.66$ mm is observed. Figure 9(b) shows that in the homogeneous mixture the distance between the two peak pressure positions is equal to the cell length of $w_0 = 1.66$ mm. When the detonation propagates into the first inhomogeneous region 1– with relatively low concentration of H_2/O_2 , the shock pressure decreases and the original cellular structure gradually disappears. In region 1+, two local explosions occur around $(x, y) = (6.6, 0.8$ cm) and $(6.7, 0.3$ cm), as shown in figure 9(a). Furthermore, the peak shock pressure is recovered as shown in figure 9(b).

Along the line $y = 0.6$ cm, [figure 9\(b\)](#) shows that the first local explosion occurs around $x = 7.25$ cm, where the local peak shock pressure appears. From region 1+ to 2+, detonation reinitiation happens. In region 3–, the shock pressure decreases again and the cellular structure tends to disappear, which is similar to the observation in region 1–. As the detonation propagates into region 3+, a much stronger second local explosion occurs, resulting in an overdriven detonation whose peak pressure is above 50 atm. Then, the large cellular structure with $\lambda_1 \approx 9.6$ mm and $w_1 \approx 15.8$ mm is formed due to the regular movement of secondary triple points. Within the large-scale cellular structure are substructures with $\lambda_0 \approx 0.833$ mm and $w_0 \approx 1.66$ mm, which are due to the movement of the original triple points as in the homogeneous mixture. [Figure 9\(a\)](#) shows that the strong collision between secondary triple points occurs in regions 3+, 5+, 7+, etc. Therefore, quasi-steady double cellular structures appear in the inhomogeneous mixture after a transition region. Such interesting cellular structure was also obtained by Radulescu & Maxwell (2011) in their study on detonation propagation across staggered cylinders and also in our previous study (Wang *et al.* 2021) on detonation propagation across inert layers.

To further visualize and interpret the detonation reinitiation and the formation of double cellular structure in the inhomogeneous mixture, in [figure 10](#) we plot the evolution of pressure, temperature and density distributions for the same case of $L = 8$ mm and $a = 0.3$. At $t = 29.1$ μs , the detonation is still in the homogenous region with $x \leq 6$ cm and the original triple points are observed. At $t = 31.1$ μs , the transmitted shock is in region 1– ($6.0 \leq x \leq 6.4$ cm) and it decouples from the reaction zone. At $t = 33.1$ μs , the mixture in region 1+ ($6.4 \leq x \leq 6.8$ cm) with relatively high reactivity is compressed by the transmitted shock and consequently local explosions are induced. Meanwhile, as the transmitted shock propagates into the inhomogeneous mixture, it interacts with the density gradient, which generates Richtmyer–Meshkov instabilities and results in the interaction of the transverse shock waves (Radulescu, Sharpe & Law 2007; Ng *et al.* 2015). The collisions between the transverse shock waves also induce local explosions. As the local explosions propagate outwards, a global explosion forms at $t = 34.1$ μs and then detonation reinitiation is successfully achieved with an irregular cellular structure, as shown in [figure 9\(a\)](#). As the detonation propagates forward, decoupling and coupling between the leading shock and reaction zone occur alternately in regions with lower and higher chemical reactivity.

[Figure 10](#) shows that shock–reaction coupling occurs in region 2+ at $t = 36.9$ μs , while decoupling occurs in region 3– at $t = 39.1$ μs . This corresponds to the transition process. After the transition, the secondary explosions are shown to occur in region 3+ at $t = 41.1$ μs . The original and secondary triple points coexist at $t = 50.1$ μs , which generates the double cellular structures. Eventually, a quasi-steady detonation with double cellular structure propagates in the inhomogeneous mixture. The length of the large-scale cell is equal to the wavelength of the sinusoidal distribution of reactant concentration.

3.2.2. Effects of mixture composition and concentration distribution

The above results are for a stoichiometric H_2/air mixture without nitrogen dilution (i.e. $s = 3.76$ in (2.1)). As mentioned previously, the induction length increases from $l_i = 0.19$ mm to $l_i = 1.25$ mm for the nitrogen-diluted mixture (i.e. $s = 7$ in (2.1)). Therefore, the cell size increases greatly for the nitrogen-diluted mixture (see [table 1](#)).

[Figure 11](#) shows the numerical soot foils for detonation propagation in a nitrogen-diluted mixture with a fixed amplitude of $a = 0.3$ but different wavelengths of $L = 1, 2$ and 4 mm. The inhomogeneous region starts at $x_0 = 30$ cm (i.e. $x_0 = 240l_i$, where l_i is the induction length for the nitrogen-diluted mixture). For the homogeneous mixture, the cell size is

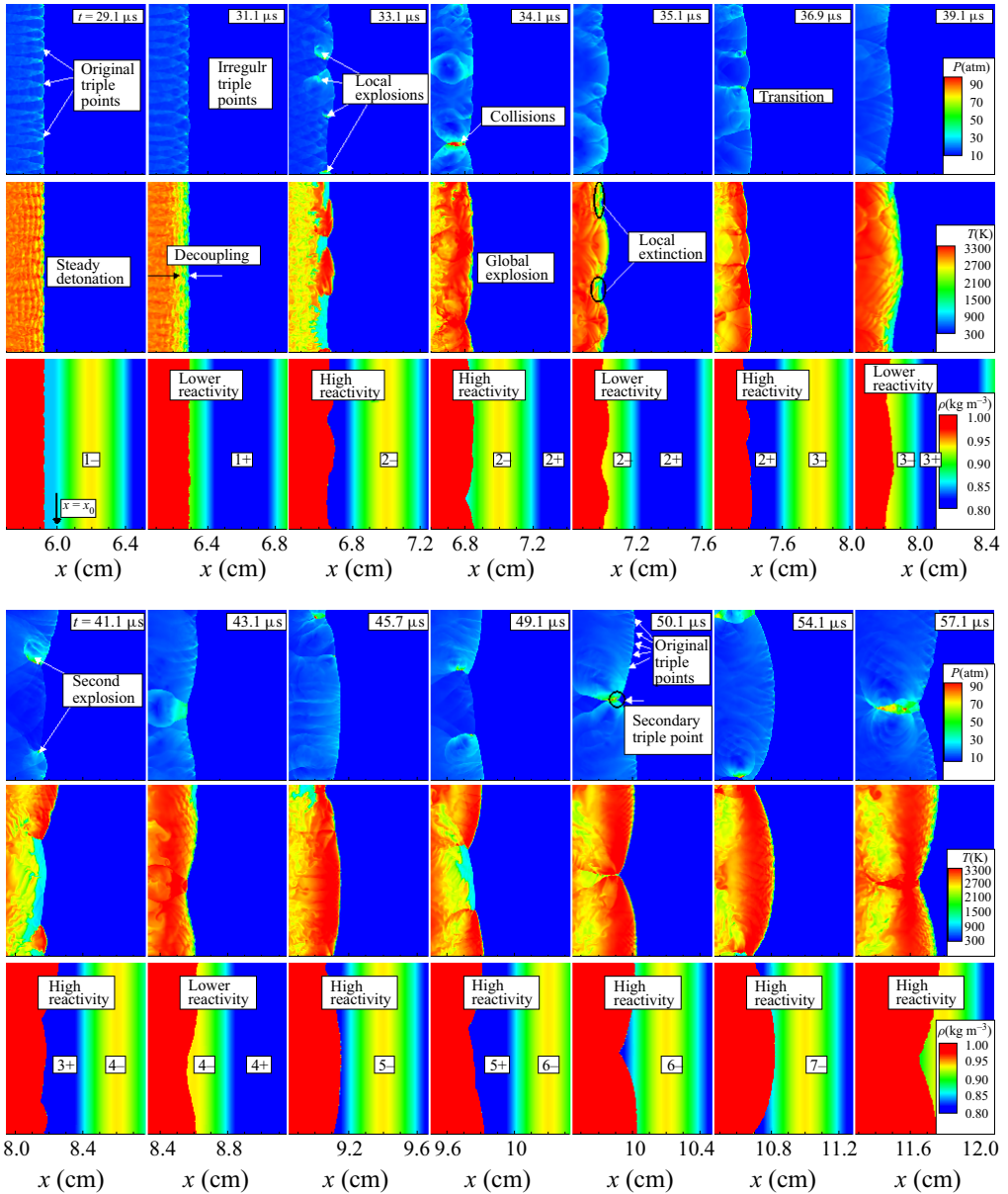


Figure 10. Evolution of pressure P (top), temperature T (middle) and density ρ (bottom) contours for $L=8$ mm and $a=0.3$ in mixture 1.

$\lambda_0 = 2.5$ mm, which is much larger than $\lambda_0 = 0.833$ mm for H_2/air without nitrogen dilution. For the inhomogeneous mixture, the cell size is shown to increase gradually with the wavelength. For $L=4$ mm, the cell size is about $\lambda=5$ mm, which is two times λ_0 . Such change is similar to that for a stoichiometric H_2/air mixture without nitrogen dilution (see figure 8). The comparison in cell sizes for mixtures without and with nitrogen dilution is shown in figure 13.

Besides the sine wave distribution of the mixture composition shown in figure 2, we also consider the square wave distribution, which is depicted in figure 12(a). The corresponding

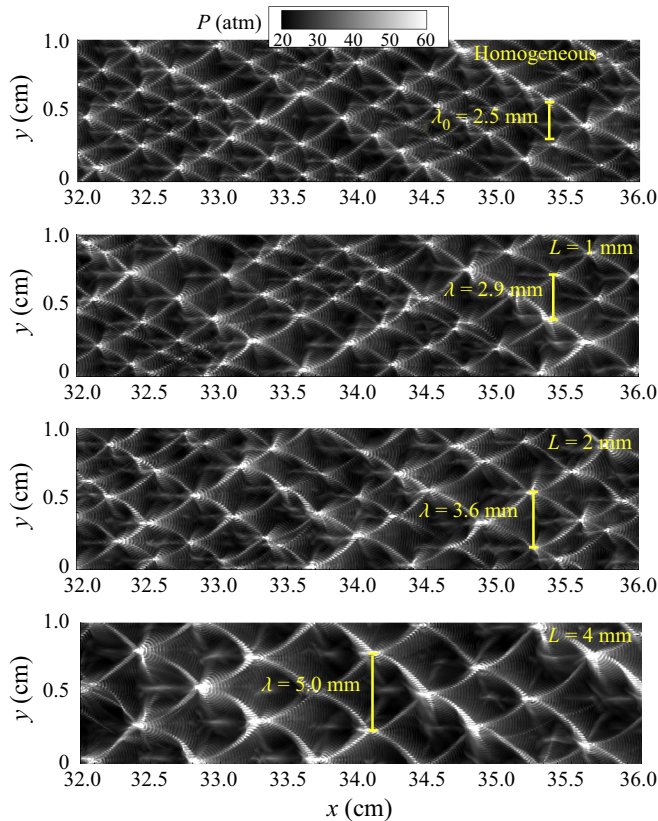


Figure 11. Numerical soot foils for a fixed amplitude of $a = 0.3$ and different wavelengths of $L = 1, 2$ and 4 mm in stoichiometric nitrogen-diluted mixture (i.e. mixture 2) with sinusoidal distribution. The results for the homogenous mixture (i.e. $a = 0$) are displayed together for comparison.

results are shown in [figure 12\(b\)](#) for a stoichiometric H_2 /air mixture without nitrogen dilution (i.e. $s = 3.76$ in (2.1)). The comparison among results shown in [figures 12\(b\)](#) and [7](#) indicates that sine wave and square wave distributions of the mixture composition have qualitatively similar effects. Specifically, for $a = 0.3$ a quasi-steady large cellular structure is observed after a transition region; while for $a = 0.5$, detonation quenching occurs in the inhomogeneous mixture. Quantitatively, the critical amplitude for the square wave distribution is smaller than that for the sine wave distribution of reactant concentration. This is consistent with previous results in [Kuznetsov *et al.* \(1998\)](#) and [Boulal *et al.* \(2016\)](#) that a smaller concentration gradient (corresponding to the sine wave distribution) is more favourable to detonation propagation, while a larger concentration gradient (corresponding to the square wave distribution) is more likely to induce detonation quenching.

3.2.3. Large cell size, quenching condition and detonation speed deficit

The above results show that for mixtures both without and with nitrogen dilution and for both sinusoidal and square wave distributions, there exists a quasi-steady large cellular structure after a transition region; otherwise, the detonation quenches in the inhomogeneous mixture. To quantify the properties of detonation propagation in inhomogeneous mixtures, here we study the change of large-scale cell size, critical amplitude, transition distance and detonation speed deficit.

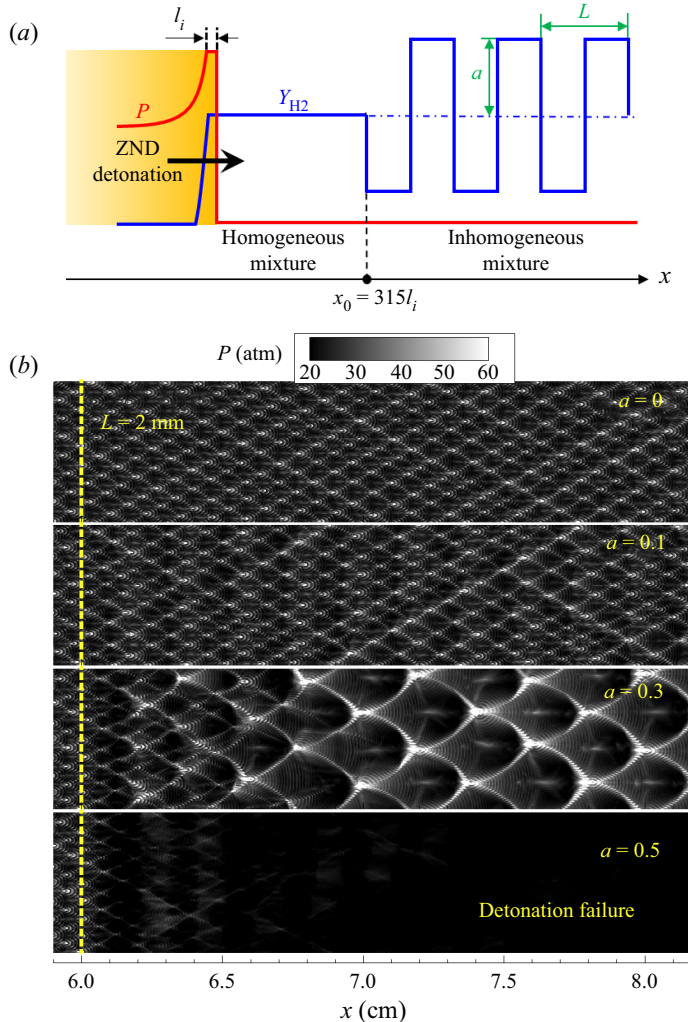


Figure 12. (a) Schematic of the initial pressure and hydrogen mass fraction distributions for the case with square wave distribution of the mixture composition. (b) Numerical soot foils for a fixed period of $L = 2$ mm and different amplitudes of $a = 0, 0.1, 0.3$ and 0.5 in a stoichiometric H_2 /air mixture (i.e. in mixture 1) with square wave distribution of the mixture composition.

Figure 13 displays the change of the normalized large cell size, λ/λ_0 , versus the normalized wavelength, L/λ_0 . Here, λ_0 is the cell size for the corresponding homogeneous $H_2/O_2/N_2$ mixture. For the H_2 /air mixture without nitrogen dilution, λ/λ_0 is shown to linearly increase with L/λ_0 , and nearly identical results are observed for the distributions of sine wave (figure 2), square wave (figure 12a) and inert layer (figure 1d) (Wang *et al.* 2021) distributions. This indicates that the large cell size is proportional to the wavelength of the mixture composition distribution. This is reasonable since the large cellular structure is mainly induced by periodic detonation reinitiation, as interpreted by figures 9 and 10. For the nitrogen-diluted mixture, the normalized large cell size is also linearly proportional to the normalized wavelength. Therefore, the change of the large cell size is independent of mixture composition and profile of the periodic gradient in reactant concentration.

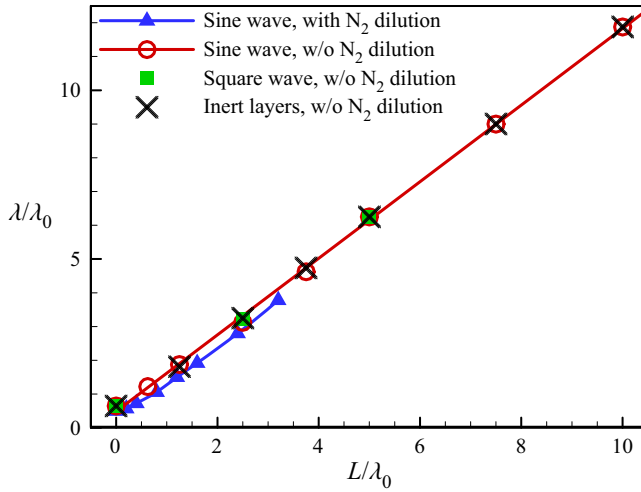


Figure 13. Change of the normalized large cell size, λ/λ_0 , with the normalized wavelength, L/λ_0 , for different mixture compositions and concentration distributions (for inert layers, L is the spacing between two consecutive inert layers).

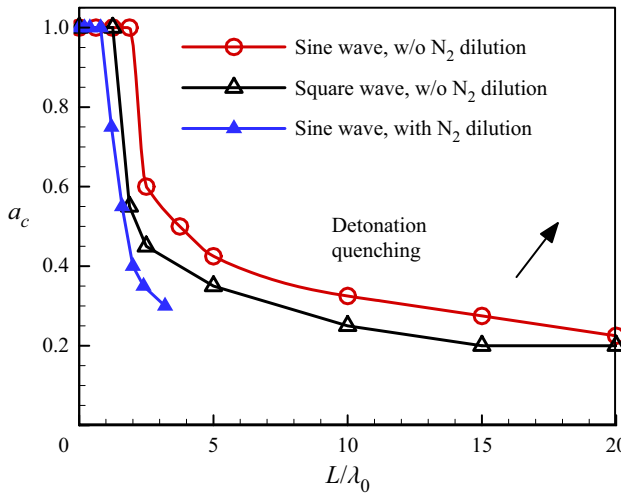


Figure 14. Change of the critical amplitude, a_c , with the normalized wavelength, L/λ_0 , for different mixture compositions and concentration distributions. Detonation quenching occurs for $a > a_c$.

It is shown in figures 7 and 12(b) that successful detonation propagation in the inhomogeneous mixture is achieved only for an amplitude below some critical value. The critical amplitudes for different mixture compositions and concentration distributions are compared in figure 14. The critical amplitude is shown to decrease monotonically with the increase of the normalized wavelength. This is because a larger wavelength corresponds to a broader region with high nitrogen concentration and thus the detonation can be quenched more easily. It is also observed that the square wave distribution of reactant concentration always has a lower critical amplitude than the sine wave distribution. This was explained in the previous subsection and is due to the relatively large concentration gradient of the square wave distribution.

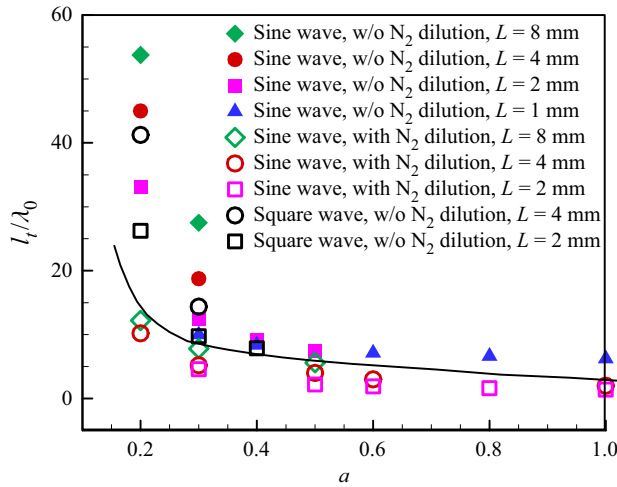


Figure 15. Change of the normalized transition distance, l_t/λ_0 , with the amplitude, a , for different mixture compositions and concentration distributions. The line separates results for mixtures without and with nitrogen dilution.

Figure 15 summarizes the change of normalized transition distance versus amplitude. With an increase of the amplitude, the normalized transition distance decreases monotonically. At lower amplitude, the detonation will not be quenched in the region with relatively lower reactant concentration, and thereby a smooth transition to the quasi-steady large cellular structure requires a relatively longer transition distance. On the contrary, at higher amplitude, the detonation can be quenched in the regions with low reactivity and reinitiation can occur afterwards, as shown in figures 9 and 10. An abrupt transition to the quasi-steady large cellular structure then requires relatively shorter transition distance. For a fixed amplitude, the normalized transition distance is shown to increase with the wavelength. This is because for a longer wavelength the large-scale cell size increases (see figures 8, 11 and 13) and the adjacent triple points of the original cells need more collisions to transform into secondary triple points. Moreover, the solid line in figure 15 indicates that the normalized transition distance becomes smaller when nitrogen dilution is introduced. The latter is due to the fact that $\lambda_0 = 2.5$ mm for the nitrogen-diluted mixture is much larger than $\lambda_0 = 0.833$ mm for the mixture without nitrogen dilution and detonation transition in an inhomogeneous mixture is therefore achieved more easily with nitrogen dilution.

The effects of the mixture composition and concentration distribution on the averaged detonation propagation speed in inhomogeneous mixtures were also examined. The results are summarized in figure 16, in which V_{CJ} is the CJ detonation speed of the homogeneous mixture and V_{AVG} is the averaged detonation speed in the quasi-steady region (i.e. after the transition region) of the inhomogeneous mixture. Since averaged fuel concentration in the inhomogeneous mixture is the same as in the homogeneous mixture (see (2.1)), V_{AVG} is close to V_{CJ} . Nevertheless, the non-uniform distribution of the mixture composition results in a minor detonation speed deficit, which is within 3% of the CJ value. Figure 16 shows that the deficit increases with the wavelength L and amplitude a . For a fixed normalized wavelength of $L/\lambda_0 = 20$, the value of V_{AVG}/V_{CJ} decreases from 98.6% for $a = 0.2$ to 97.3% for $a = 0.3$. For a fixed amplitude of $a = 0.3$, the value of V_{AVG}/V_{CJ} decreases from 99.5% for $L/\lambda_0 = 1.25$ to 97.3% for $L/\lambda_0 = 20$ in the H_2 /air mixture with sinusoidal distribution. Moreover, the square wave distribution and nitrogen dilution further decrease

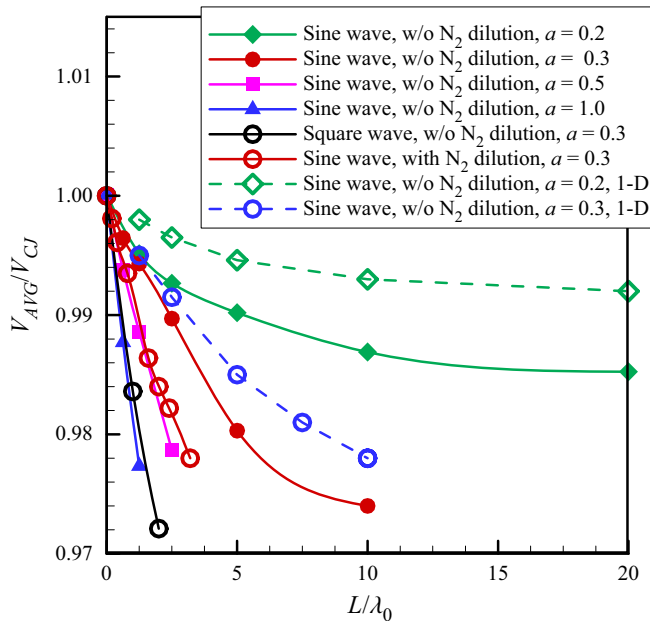


Figure 16. Change of the normalized averaged detonation propagation speed, V_{AVG}/V_{CJ} , with the normalized wavelength, L/λ_0 , for different mixture compositions and concentration distributions.

the averaged detonation propagation speed. This is because the detonation quenches more easily in inhomogeneous mixtures with square wave distribution of reactants and the detonation intensity becomes weaker after nitrogen dilution. Furthermore, the results for 2-D simulations are in agreement with those of the 1-D simulations as shown in figure 6.

The above detonation speed deficit can be interpreted through comparing the amount of unburned hydrogen left behind the detonation, $Y_{H_2,Left}$, in the inhomogeneous mixture with that in the homogenous mixture, $Y_{H_2,Left,Hom}$. Here $Y_{H_2,Left}$ is calculated in the zone from x_0 to detonation front, in which the condition $Y_{H_2} > 0.002$ was satisfied. It is found that more unburned hydrogen is left behind the detonation in the inhomogeneous than in the homogenous mixture case, which is the cause of the detonation speed deficit shown in figure 16. Figure 17 plots the change of the normalized averaged detonation propagation speed versus the normalized unburned hydrogen mass fraction for different mixture compositions and concentration distributions. The solid line represents the theoretical CJ detonation speed calculated based on reactant concentration. Good agreement between theoretical and simulation results can be observed. This demonstrates that the detonation speed deficit in the inhomogeneous mixture is due to the amount of unburned fuel left behind the detonation with cellular structure.

Figures 13–17 quantitatively analyse the change of cell size, critical amplitude, transition distance and detonation speed deficit and good agreement is achieved for both mixture 1 without nitrogen dilution and mixture 2 with nitrogen dilution and for both sinusoidal and square wave distributions. This indicates that detonation propagating through inhomogeneous mixtures can be accurately simulated in the present study.

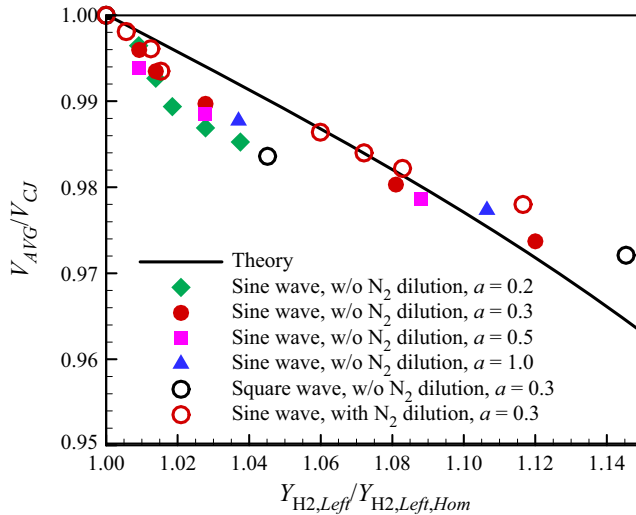


Figure 17. Change of the normalized averaged detonation propagation speed, V_{AVG}/V_{CJ} , with the normalized unburned hydrogen mass fraction, $Y_{H_2,Left}/Y_{H_2,Left,Hom}$, for different mixture compositions and concentration distributions.

3.3. Comparison of 1-D and 2-D detonation propagation

The interaction of transverse waves is critical for detonation reinitiation in 2-D cases since the transverse waves combine with the leading compression shock in triple points, which induce autoignition/local explosion, as demonstrated in figure 10. However, in 1-D cases the autoignition is induced only by the leading shock compression (see figure 4). The absence of transverse waves in the 1-D cases results in a much longer duration and thereby distance for detonation reinitiation. In this respect, the multidimensional effect (which allows the existence of transverse waves) can greatly promote detonation reinitiation. Figure 10 shows that there are several unreacted pockets when the detonation propagates in the inhomogeneous mixture with periodic gradient in reactant concentration. These unreacted pockets reduce the total heat release and increase the unburned reactant concentration in the burned products. Though a similar phenomenon is also observed for 1-D simulations, the amount of unburned reactant in the 1-D cases is much less than that in the 2-D cases. In this respect, the multidimensional effect (which results in an increased amount of unburned reactant) prevents the detonation reinitiation. The inhibiting effects due to unburned reactants are stronger than the promoting effects due to transverse waves. Consequently, the 2-D cases exhibit smaller critical amplitude and wavelength for the periodic mixture composition distribution than the 1-D cases. Moreover, the averaged detonation propagation speed deficit in the 2-D cases is slightly larger than that in the 1-D cases due to a larger amount of unburned reactant in the multidimensional detonation structure.

In 1-D cases, a double periodic fluctuation of the peak pressure after the shock is observed (see figures 3 and 5). Similarly, a double cellular structure, consisting of substructures and a large-scale structure, is observed in 2-D cases (see figures 8 and 9). Therefore, the 1-D and 2-D cases exhibit similarity in the change of the original mode of detonation propagation in inhomogeneous mixtures with periodic gradient in reactant concentration. In inhomogeneous mixtures, the detonation speed, the number of triple points and the cellular structure adjust to the local mixture composition.

Therefore, the quasi-steady detonation propagation with double periodic fluctuations of peak shock pressure and double cellular structure is observed after a transition distance in both 1-D and 2-D cases.

4. Conclusions

Detonation propagation in inhomogeneous $H_2/O_2/N_2$ mixtures with a periodic gradient in reactant concentration were studied through 1-D and 2-D simulations considering detailed chemistry and transport. Two types of mixtures, hydrogen/air without and with nitrogen dilution, and two types of non-uniform mixture composition distribution, periodic sine wave and square wave, were considered. It was observed that a detonation can be completely quenched in the inhomogeneous mixture when the amplitude or wavelength of the periodic mixture composition distribution is above certain critical threshold values. The critical amplitude decreases monotonically with the increase of wavelength. Further, the square wave distribution of reactant concentration always has a lower critical amplitude than the sine wave distribution. For certain amplitude and wavelength values below their critical thresholds, detonation quenching and reinitiation were found to occur alternately in the inhomogeneous mixtures. Successful reinitiation can be triggered by local autoignition and explosion due to collision of transverse shock waves. There exists a double period of the leading shock pressure propagation for 1-D simulations and a double cellular structure consisting of a large-scale structure and smaller substructures, respectively due to the movement of the original and secondary triple points for 2-D simulations. The normalized large-scale cell size was found to be linearly proportional to the normalized wavelength but independent of the amplitude of non-uniform mixture composition distribution. Furthermore, a small detonation speed deficit in the inhomogeneous mixture was found and could be attributed to the amount of unburned fuel left behind the detonation with cellular structure.

This work reported two new physical phenomena for detonation propagation in inhomogeneous mixtures with periodic reactant concentration gradient: the alternately occurring detonation quenching and reinitiation and the double cellular structure consisting of a large-scale structure and smaller substructures. These two phenomena were interpreted in detail in this work. Although no experimental validation or general theory can yet be provided, this work is a first step towards a better understanding of these two phenomena. While only hydrogen has been considered, it is expected that similar phenomena would be observed for other fuels such as ethylene and *n*-decane. The influence of fuels and thermal conditions will be investigated in future works.

Supplementary material. Supplementary material is available at <https://doi.org/10.1017/jfm.2022.1074>.

Acknowledgements. We thank the anonymous reviewers for their comments/suggestions which helped to improve this paper. Y.W. and Z.C. thank Professor Xiaocheng Mi at Eindhoven University of Technology and Dr Pengfei Yang and Mr Jie Sun at Peking University for helpful discussions. The simulations were conducted on the High Performance Computing Platform of the Center for Life Science at PKU and on the Tianhe-2A supercomputer in Guangzhou, China.

Funding. This work was supported by the National Natural Science Foundation of China (no. 52176096).

Declaration of interests. The authors report no conflict of interest.

Author ORCIDs.

 Ralf Deiterding <https://orcid.org/0000-0003-4776-8183>;

 Zheng Chen <https://orcid.org/0000-0001-7341-6099>.

REFERENCES

- BJERKETVEDT, D., SONJU, O.K. & MOEN, I.O. 1986 The influence of experimental condition on the reinitiation of detonation across an inert region. *Prog. Astronaut. Aeronaut.* **106**, 109–130.
- BOECK, L.R., BERGER, F.M., HASSLBERGER, J. & SATTELMAYER, T. 2015 Detonation propagation in hydrogen-air mixtures with transverse concentration gradients. *Shock Waves* **26** (2), 181–192.
- BOULAL, S., VIDAL, P. & ZITOUN, R. 2016 Experimental investigation of detonation quenching in non-uniform compositions. *Combust. Flame* **172**, 222–233.
- BOULAL, S., VIDAL, P., ZITOUN, R., MATSUMOTO, T. & MATSUO, A. 2018 Experimental investigation on detonation dynamics through a reactivity sink. *Combust. Flame* **196**, 11–25.
- BROWN, P.N., BYRNE, G.D. & HINDMARSH, A.C. 1989 VODE: a variable-coefficient ODE solver. *SIAM J. Sci. Stat. Comput.* **10**, 1038–1051.
- CALHOON, W.H. & SINHA, N. 2005 Detonation wave propagation in concentration gradients. In *43rd AIAA Aerospace Sciences Meeting, Nevada. AIAA Paper 2005-1167*.
- CHEN, Z. 2010 Effects of radiation and compression on propagating spherical flames of methane/air mixtures near the lean flammability limit. *Combust. Flame* **157** (12), 2267–2276.
- CHEN, Y.L., LIU, X.Y. & WANG, J.P. 2019 Mode switching in 2-dimensional continuous detonation chambers with discrete injectors. In *Proceedings of the 27th International Colloquium on the Dynamics of Explosions and Reactive Systems, Beijing*.
- DAI, P. & CHEN, Z. 2015 Supersonic reaction front propagation initiated by a hot spot in n-heptane/air mixture with multistage ignition. *Combust. Flame* **162** (11), 4183–4193.
- DAI, P. & CHEN, Z. 2019 Effects of NOx addition on autoignition and detonation development in DME/air under engine-relevant conditions. *Proc. Combust. Inst.* **37** (4), 4813–4820.
- DAIMON, Y. & MATSUO, A. 2007 Unsteady features on one-dimensional hydrogen-air detonations. *Phys. Fluids* **19**, 116101.
- DEITERDING, R. 2009 A parallel adaptive method for simulating shock-induced combustion with detailed chemical kinetics in complex domains. *Comput. Struct.* **87** (11–12), 769–783.
- DEITERDING, R. 2011 High-resolution numerical simulation and analysis of mach reflection structures in detonation waves in low-pressure H₂-O₂-Ar mixtures: a summary of results obtained with the adaptive mesh refinement framework AMROC. *J. Combust.* **2011**, 738969.
- ETTNER, F., VOLLMER, K.G. & SATTELMAYER, T. 2013 Mach reflection in detonations propagating through a gas with a concentration gradient. *Shock Waves* **23** (3), 201–206.
- FUJII, J., KUMAZAWA, Y., MATSUO, A., NAKAGAMI, S., MATSUOKA, K. & KASAHARA, J. 2017 Numerical investigation on detonation velocity in rotating detonation engine chamber. *Proc. Combust. Inst.* **36** (2), 2665–2672.
- GAATHAUG, A.V., VAAGSAETHER, K. & BJERKETVEDT, D. 2017 Detonation failure in stratified layers-the influence of detonation regularity. In *Proceedings of the 26th International Colloquium on the Dynamics of Explosions and Reactive Systems, Boston*.
- GAVRILENKO, T.P., KRASNOV, A.N. & NIKOLAEV, Y.A. 1982 Transfer of a gas detonation through an inert gas ‘plug’. *Combust. Explos. Shock Waves* **18**, 240–244.
- GOODWIN, D., MOFFAT, H.K. & SPETH, R.L. 2016 Cantera: An Object-oriented Software Toolkit for Chemical Kinetics, Thermodynamics, and Transport Processes. Version 2.2.1.
- GRUNE, J., SEMPET, K., FRIEDRICH, A., KUZNETSOV, M. & JORDAN, T. 2017 Detonation wave propagation in semi-confined layers of hydrogen-air and hydrogen-oxygen mixtures. *Intl J. Hydrogen Energy* **42** (11), 7589–7599.
- HAN, W., GAO, Y. & LAW, C.K. 2017 Flame acceleration and deflagration-to-detonation transition in micro-and macro-channels: An integrated mechanistic study. *Combust. Flame* **176**, 285–298.
- HAN, W., WANG, C. & LAW, C.K. 2019 Role of transversal concentration gradient in detonation propagation. *J. Fluid Mech.* **865**, 602–649.
- HOUIM, R.W. & FIEVISOHN, R.T. 2017 The influence of acoustic impedance on gaseous layered detonations bounded by an inert gas. *Combust. Flame* **179**, 185–198.
- HUANG, C., QI, C. & CHEN, Z. 2019 Non-uniform ignition behind a reflected shock and its influence on ignition delay measured in a shock tube. *Shock Waves* **29** (7), 957–967.
- ISHII, K. & KOJIMA, M. 2007 Behavior of detonation propagation in mixtures with concentration gradients. *Shock Waves* **17** (1–2), 95–102.
- ISHII, K. & SEKI, K. 2017 A study on suppression of detonation propagation by inert gas injection. In *Proceedings of the 26th International Colloquium on the Dynamics of Explosions and Reactive Systems, Boston*.
- KESSLER, D.A., GAMEZO, V.N. & ORAN, E.S. 2012 Gas-phase detonation propagation in mixture composition gradients. *Phil. Trans. A Math. Phys. Engng Sci.* **370** (1960), 567–596.

- KHODADADI AZADBONI, R., HEIDARI, A., BOECK, L.R. & WEN, J.X. 2019 The effect of concentration gradients on deflagration-to-detonation transition in a rectangular channel with and without obstructions – a numerical study. *Intl J. Hydrogen Energy* **44** (13), 7032–7040.
- KUZNETSOV, M.S., ALEKSEEV, V.I., DOROFEEV, S.B., MATSUKOV, I.D. & BOCCIO, J.L. 1998 Detonation propagation, decay, and reinitiation in nonuniform gaseous mixtures. *Proc. Combust. Inst.* **27**, 2241–2247.
- KUZNETSOV, M.S., DOROFEEV, S.B., EFIMENKO, A.A., ALEKSEEV, V.I. & BREITUNG, W. 1997 Experimental and numerical studies on transmission of gaseous detonation to a less sensitive mixture. *Shock Waves* **7**, 297–304.
- LI, J., LAI, W.H., CHUNG, K. & LU, F.K. 2008 Experimental study on transmission of an overdriven detonation wave from propane/oxygen to propane/air. *Combust. Flame* **154** (3), 331–345.
- LI, J., MI, X. & HIGGINS, A.J. 2015 Effect of spatial heterogeneity on near-limit propagation of a pressure-dependent detonation. *Proc. Combust. Inst.* **35** (2), 2025–2032.
- LI, J., ZHAO, Z., KAZAKOV, A. & DRYER, F.L. 2004 An updated comprehensive kinetics model of hydrogen combustion. *Intl J. Chem. Kinet.* **36**, 566–575.
- LIEBERMAN, D.H. & SHEPHERD, J.E. 2007a Detonation interaction with a diffuse interface and subsequent chemical reaction. *Shock Waves* **16** (6), 421–429.
- LIEBERMAN, D.H. & SHEPHERD, J.E. 2007b Detonation interaction with an interface. *Phys. Fluids* **19**, 096101.
- LU, F.K. & BRAUN, E.M. 2014 Rotating detonation wave propulsion: experimental challenges, modeling, and engine concepts. *J. Propul. Power* **30**, 1125–1142.
- MA, W.J., WANG, C. & HAN, W.H. 2020 Effect of concentration inhomogeneity on the pulsating instability of hydrogen-oxygen detonations. *Shock Waves* **30** (7-8), 703–711.
- MAXWELL, B. & MELGUIZO-GAVILANES, J. 2019 Origins of turbulent mixing behind detonation propagation into reactive–inert gas interfaces. In *Proceedings of the 27th International Colloquium on the Dynamics of Explosions and Reactive Systems, Beijing*.
- MI, X., HIGGINS, A.J., NG, H.D., KIYANDA, C.B. & NIKIFORAKIS, N. 2017a Propagation of gaseous detonation waves in a spatially inhomogeneous reactive medium. *Phys. Rev. Fluids* **2** (5), 053201.
- MI, X.C., MICHAEL, L., NIKIFORAKIS, N. & HIGGINS, A.J. 2019 Shock-to-detonation transition in nitromethane with spatially non-uniform distributions of air-filled cavities. In *Proceedings of the 27th International Colloquium on the Dynamics of Explosions and Reactive Systems, Beijing*.
- MI, X., TIMOFEEV, E.V. & HIGGINS, A.J. 2017b Effect of spatial discretization of energy on detonation wave propagation. *J. Fluid Mech.* **817**, 306–338.
- NG, H.D., KIYANDA, C.B., MORGAN, G.H. & NIKIFORAKIS, N. 2015 The influence of high-frequency instabilities on the direct initiation of two-dimensional gaseous detonations. In *Proceedings of the 25th International Colloquium on the Dynamics of Explosions and Reactive Systems, Leeds*.
- PEACE, J.T. & LU, F.K. 2017 Study of shock wave transmission by detonation wave interaction with contact discontinuity. In *55th AIAA Aerospace Sciences Meeting, Texas*.
- PEACE, J.T. & LU, F.K. 2018 Detonation-to-shock wave transmission at a contact discontinuity. *Shock Waves* **28** (5), 981–992.
- PRAKASH, S. & RAMAN, V. 2019 Detonation propagation through inhomogeneous fuel-air mixtures. In *Proceedings of the 27th International Colloquium on the Dynamics of Explosions and Reactive Systems, Beijing*.
- PRESLES, H.N., DESBORDES, D., GUIRARD, M. & GUERRAUD, C. 1996 Gaseous nitromethane and nitromethane-oxygen mixtures: a new detonation structure. *Shock Waves* **6** (2), 111–114.
- QI, C. & CHEN, Z. 2017 Effects of temperature perturbation on direct detonation initiation. *Proc. Combust. Inst.* **36** (2), 2743–2751.
- QI, C., DAI, P., YU, H. & CHEN, Z. 2017 Different modes of reaction front propagation in n-heptane/air mixture with concentration non-uniformity. *Proc. Combust. Inst.* **36** (3), 3633–3641.
- RADULESCU, M.I. & MAXWELL, B.M. 2011 The mechanism of detonation attenuation by a porous medium and its subsequent re-initiation. *J. Fluid Mech.* **667**, 96–134.
- RADULESCU, M.I., SHARPE, G.J. & LAW, C.K. 2007 Effect of cellular instabilities on the blast initiation of weakly unstable detonations. In *Proceedings of the 21st International Colloquium on the Dynamics of Explosions and Reactive Systems, Poitiers*.
- REYNAUD, M., VIROT, F. & CHINNAYYA, A. 2017 A computational study of the interaction of gaseous detonations with a compressible layer. *Phys. Fluids A* **29**, 056101.
- TAILEB, S., MELGUIZO-GAVILANES, J. & CHINNAYYA, A. 2019 Chemistry modeling effects on the interaction of a gaseous detonation with an inert layer. In *Proceedings of the 27th International Colloquium on the Dynamics of Explosions and Reactive Systems, Beijing*.

- TANG, K.C., LEE, J.H.S., NG, H.D. & MI, X.C. 2019a Detonation transmission across an inert gap. In *Proceedings of the 27th International Colloquium on the Dynamics of Explosions and Reactive Systems, Beijing*.
- TANG, K.C., LEE, J.H.S., NG, H.D. & MI, X.C. 2019b Transmission of cellular detonation waves across a density/temperature interface. In *Proceedings of the 27th International Colloquium on the Dynamics of Explosions and Reactive Systems, Beijing*.
- TANG, K.C., MI, X.C., LEE, J.H.S. & NG, H.D. 2018 Transmission of a detonation across a density interface. *Shock Waves* **28** (5), 967–979.
- TANG, K.C., MI, X.C., LEE, J.H.S., TENG, H.H. & NG, H.D. 2017 Numerical study of gaseous detonation propagation across a density interface. In *Proceedings of the 26th International Colloquium on the Dynamics of Explosions and Reactive Systems, Boston*.
- TEODORCZYK, A. & BENOAN, F. 1996 Interaction of detonation with inert gas zone. *Shock Waves* **6**, 211–223.
- THOMAS, G.O., SUTTON, P. & EDWARDS, D.H. 1991 The behavior of detonation waves at concentration gradients. *Combust. Flame* **84**, 312–322.
- WANG, Y., HAN, W., DEITERDING, R. & CHEN, Z. 2018 Effects of disturbance on detonation initiation in $\text{H}_2/\text{O}_2/\text{N}_2$ mixture. *Physical Review Fluids* **3**, 123201.
- WANG, Y., HUANG, C., DEITERDING, R., CHEN, H. & CHEN, Z. 2021 Propagation of gaseous detonation across inert layers. *Proc. Combust. Inst.* **38** (3), 3555–3563.
- ZELDOVICH, Y.B. 1980 Regime classification of an exothermic reaction with nonuniform initial conditions. *Combust. Flame* **39**, 211–214.
- ZHENG, W., KAPLAN, C.R., HOUIM, R.W. & ORAN, E.S. 2019 Flame acceleration and transition to detonation in methane-air mixtures with composition gradients. In *Proceedings of the 27th International Colloquium on the Dynamics of Explosions and Reactive Systems, Beijing*.